Tuning the thermal conductivity of strontium titanate through annealing treatments*

Liang Zhang(张嘹)[1], Ning Li(李宁)[1], Hui-Qiong Wang(王惠琼)[1,3,†], Yufeng Zhang(张宇锋)[1], Fei Ren(任飞)[1], Xia-Xia Liao(廖霞霞)[1], Ya-Ping Li(李亚平)[1], Xiao-Dan Wang(王小丹)[1], Zheng Huang(黄政)[1], Yang Dai(戴扬)[4], Hao Yan(鄢浩)[4], and Jin-Cheng Zheng(郑金成)[1,2,3,‡]

[1] *Collaborative Innovation Center for Optoelectronic Semiconductors and Efficient Devices, Department of Physics, Xiamen University, Xiamen* 361005, *China*

[2] *Fujian Provincial Key Laboratory of Mathematical Modeling and High-Performance Scientific Computation, Xiamen* 361005, *China*

[3] *Xiamen University Malaysia, Sepang, Selangor* 439000, *Malaysia*

[4] *Department of Chemical Engineering, School of Environmental and Chemical Engineering, Shanghai University, Shanghai* 200444, *China*

(Received 5 May 2016; revised manuscript received 2 September 2016; published online 30 November 2016)

Strontium titanate ($SrTiO_3$) is a promising n-type material for thermoelectric applications. However, its relatively high thermal conductivity limits its performance in efficiently converting heat into electrical power through thermoelectric effect. This work shows that the thermal conductivity of $SrTiO_3$ can be effectively reduced by annealing treatments, through an integrated study of laser flash measurement, scanning electron microscopy, Fourier transform infrared spectroscopy, x-ray absorption fine structure, and first-principles calculations. A phonon scattering model is proposed to explain the reduction of thermal conductivity after annealing. This work suggests a promising means to characterize and optimize the material for thermoelectric applications.

Keywords: thermal conductivity, $SrTiO_3$, annealing, phonon scattering

PACS: 66.70.−f, 81.40.Ef, 63.20.K−, 61.05.cj **DOI:** 10.1088/1674-1056/26/1/016602

1. Introduction

Thermoelectric effect can be used to directly convert heat into electrical power. The efficiency of a thermoelectric material depends on a dimensionless figure of merit defined as[1–3] $ZT = S^2\sigma T/\kappa$, where Z, T, S, σ, and κ are the figure of merit, absolute temperature, Seebeck coefficient, electrical conductivity, and thermal conductivity (which is composed of lattice part κ_l and electron part κ_e), respectively. Increasing the power factor $S^2\sigma$ and decreasing the thermal conductivity κ simultaneously lead to a higher ZT. However, these three parameters are coupled, while increasing in S often results in the suppression of σ and κ_e. One effective approach to enhance ZT is to lower the total thermal conductivity by decreasing the phonon component while maintaining the electrical conductivity.[4,5]

Metal oxides have drawn great attention as promising thermoelectric materials due to their non-toxicity, abundance, and stability. Among them, $SrTiO_3$ is regarded as one of the most promising n-type materials for thermoelectric applications. The wide band-gap perovskite oxide can be easily doped at cation Sr and Ti sites or with oxygen vacancies to form an n-type semiconductor.[6,7] The power factor of La doped $SrTiO_3$ single crystal reaches 36 $\mu W/cmK^2$ at room temperature,[7] which is comparable to the typical thermoelectric materials like SnSe,[8] and likely due to the significant contribution from the Ti d band.[9] Despite the excellent electronic properties, the lattice thermal conductivity of $SrTiO_3$ is comparatively high, which results in a relatively lower ZT. Various methods, such as nanostructuring,[10] cation doping,[11] and introduction of Sr site[12] or oxygen vacancies,[13,14] are proposed to improve the ZT of $SrTiO_3$. As a common post-treatment method,[15–19] thermal annealing in reducing atmosphere or in vacuum can generate oxygen vacancies in metal oxides and will affect their electrical and thermal properties.

In this work, the thermal transport properties (including thermal diffusivity, heat capacity, thermal conductivity) of $SrTiO_3$ are tuned by thermal annealing and measured by the laser flash method and differential scanning calorimetry. Then the structural, vibrational, and electronic properties of $SrTiO_3$ are studied by scanning electron microscopy (SEM), Fourier transform infrared spectroscopy (FTIR), and near-edge x-ray absorption fine structure (NEXAFS), respectively. We also perform first-principles calculations to compare with the experiments. A phonon scattering model is proposed to explain the reduction of thermal conductivity after annealing treatments.

*Project supported by the National Natural Science Foundation of China (Grant Nos. U1332105, 51475396, 11335006, 21103109, 21176152, and 21373137), the Natural Science Foundation of Fujian Province of China (Grant No. 2013J01026), and the Fundamental Research Funds for Central Universities of China (Grant Nos. 2013121012, 20720140517, 20720160013, and 20720160020).

†Corresponding author. E-mail: hqwang@xmu.edu.cn

‡Corresponding author. E-mail: jczheng@xmu.edu.cn

© 2017 Chinese Physical Society and IOP Publishing Ltd

2. Experiments and simulations

Commercially available single-crystalline substrates of $SrTiO_3$ (4 mm × 4 mm × 0.5 mm) were obtained from HEFEI KEJING Materials technology Co., LTD. The $SrTiO_3$ substrates were annealed at various temperatures (from 1073 K to 1473 K) either in Ar atmosphere for 24 h or under vacuum (10^{-3} Pa) for 4 h. The morphology of the samples was characterized by SEM using LEO 1530. The thermal diffusivity of the samples was measured by the laser flash method (LFA)[20] using a NETZSCH LFA457 MicroFlash apparatus with the temperature ranging from 373 K to 773 K in a nitrogen atmosphere. The specific heats C_p of the samples were characterized by differential scanning calorimetry (DSC) using a NETZSCH DSC 404 F3 Pegasus apparatus. The thermal conductivity was calculated according to the equation

$$\kappa = \alpha C_p \rho, \tag{1}$$

where α, C_p, and ρ are the thermal diffusivity, the specific heat at constant pressure, and the density, respectively.

FTIR measurements were performed by Bruker VERTEX 70v spectrometer in the far infrared region. The NEXAFS was measured at synchrotron radiation beamline 24A1 in the NSRRC. The O *K*-edge and Ti *L*-edge NEXAFS data were collected in the total electron yield (TEY) mode. The photon energy was calibrated by the binding energy of Au 4f. First principle calculations have been carried out utilizing the WIEN2k code[21] with the method of full potential linearized augmented plane wave plus local orbital (FP-LAPW+lo).[22] For the ground-state calculations, the exchange–correlation interaction was described by the Perdew–Burke–Ernzerhof generalized gradient approximation (PBE-GGA).[23] The muffin-tin radii were selected to be 2.5 a.u. for Sr, 1.87 a.u. for Ti, and 1.69 a.u. for O. The self-consistency was defined when the total energy converges less than 1 mRy and the charge converges less than 0.0005*e*.

3. Results and discussion

The temperature dependences of thermal diffusivity and specific heat of the annealed samples (treated under the vacuum pressure of 10^{-3} Pa for 4 h) where compared to those of the as-received sample, as shown in Fig. 1. The results were used to calculate the thermal conductivity of the samples (shown in Fig. 1). The annealed samples show a dramatic decrease in thermal conductivity with increasing annealing temperature. For example, the thermal conductivity of the $SrTiO_3$ sample annealed at 1473 K is 3.26 W/mK at 773 K, which is 32% lower than that of the as-received sample. According to the study of Muta,[13] the electrical conductivity of a $SrTiO_3$ sample annealed under vacuum is about $1.5 \times 10^3\ \Omega^{-1}\cdot m^{-1}$ at 373 K and gradually decreases to $1.5 \times 10^2\ \Omega^{-1}\cdot m^{-1}$ at 773 K. According to the Widemann–Franz law $\kappa_e = L_0 \sigma T$ (where L_0 is the Lorentz number and equals to 2.0×10^{-8} V^2/K^2 for a degenerated semiconductor[11]), the electronic contribution to the thermal conductivity is in the range of 0.001 W/mK to 0.01 W/mK, which is negligible comparing to the measured thermal conductivity (3–8 W/mK in the temperature range of 300–800 K). Thus, the electronic thermal conductivity can be ignored in this work, and the large suppression of thermal transport is mainly due to the decrease of the lattice thermal conductivity.

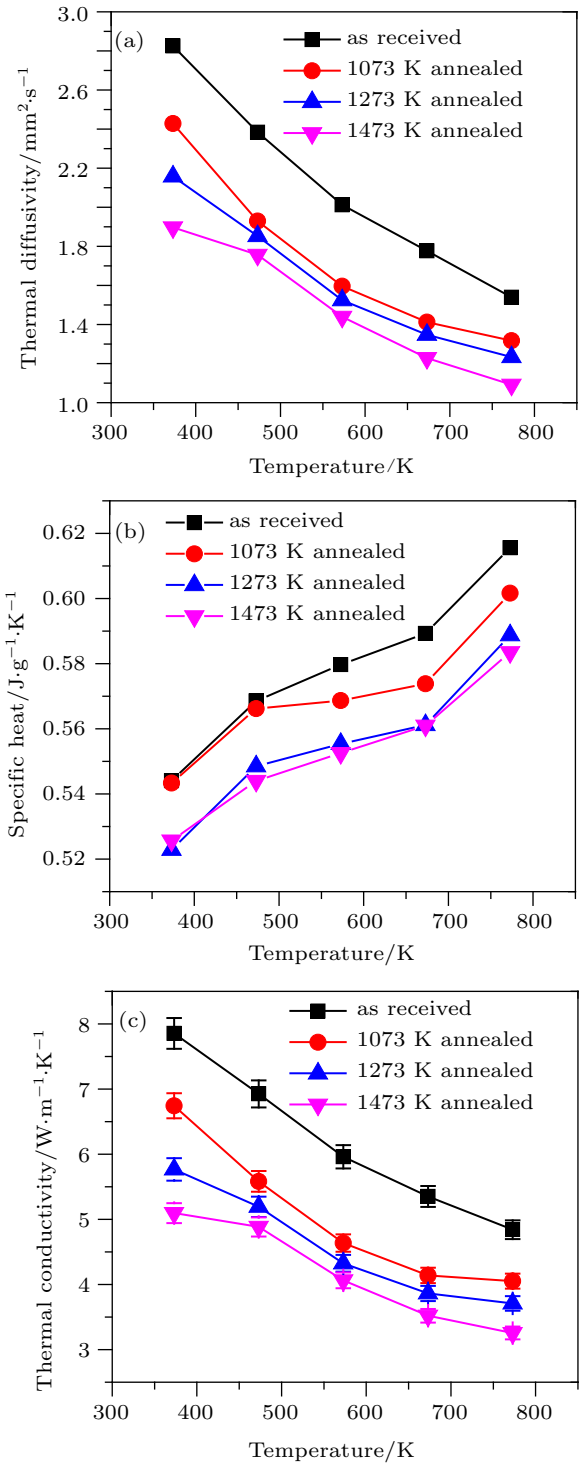


Fig. 1. (color online) Thermal conductivity of the annealed $SrTiO_3$ samples, compared with that of as-received $SrTiO_3$ sample.

In order to investigate the potential mechanism for the decrease of the lattice thermal conductivity, FTIR was employed to characterize the as-received $SrTiO_3$ sample as well as the annealed (in Ar atmosphere at 1073 K, 1173 K, and 1273 K for 24 h) samples, as shown in Fig. 2. The absorption bands consist of two features (labeled as A and B) in the range of 590–640 cm^{-1}, which originate from the Ti–O stretching vibration and assigned to the transverse optic (TO) phonon mode.[24] The existence of the two features in this range is likely due to the slight difference in Ti–O bond structures (e.g., near or away from defects). For the spectra of the as-received samples, the asymmetric shape of the two features suggests that more than one component exists in each feature, which leads to an FWHM of approximately 10 cm^{-1}. With increasing annealing temperature, the shapes of the two features become symmetric, which results in a drop of FWHM of both features (around 5 cm^{-1}). This is consistent with an earlier report, and attributes to relaxing of the strain and reordering of the $SrTiO_3$ crystal.[25] Such development in the spectral shape also implies that the Ti–O band structures gradually segregate into two distinct categories, which is consistent with the observed evolution of samples' morphology (emerging of linear dislocations in scanning microscopic images, as shown in Appendix Fig. A1). The center of feature A remains stable (around 621 ± 1 cm^{-1}), while the center of feature B increases from 606 cm^{-1} to 610 cm^{-1} with increasing annealing temperature. This suggests that feature A is more likely associated with Ti–O bonds within perfect lattice structure (without oxygen vacancies), and feature B is linked with Ti–O bonds near defects (e.g., oxygen vacancies). Furthermore, the intensity ratio (B/A) gradually increases with increasing annealing temperature, from 0.89 (as-received) to 1.2 (annealed at 1273 K), which indicates that the concentration of defects rises with increasing annealing temperature. This suggests that the annealing treatment improves the crystallinity of the samples in some regions, but leads to segregation of defects in other regions.

The crystallinity of a material correlates with its electronic structure. Hence, the NEXAFS spectra were measured for the annealed samples (treated at 1473 K under the vacuum pressure of 10^{-3} Pa for 4 h), and compared with that of the as-received sample, in order to gain more insight into the samples' properties after annealing. The O *K*-edge spectra shown in Fig. 3(a) reflect the transitions from the O 1s core level to the unoccupied O 2p (and potentially hybridized Ti 3d) conduction band. For comparison, the calculated partial densities of states (PDOS) for oxygen and titanium are presented in Fig. 3(a) as well. The peak A at 531.0 eV is likely originated from the hybridization of O p_x and p_y states with Ti t_{2g} state. The peak B (533.4 eV) is related to the hybridization of O 2p and Ti e_g states.[26] The FWHMs of the peaks are slightly enlarged after annealing, which indicates an increase of the oxygen vacancies.[27] This is likely due to the reduced symmetry caused by the presence of the oxygen vacancies.[28]

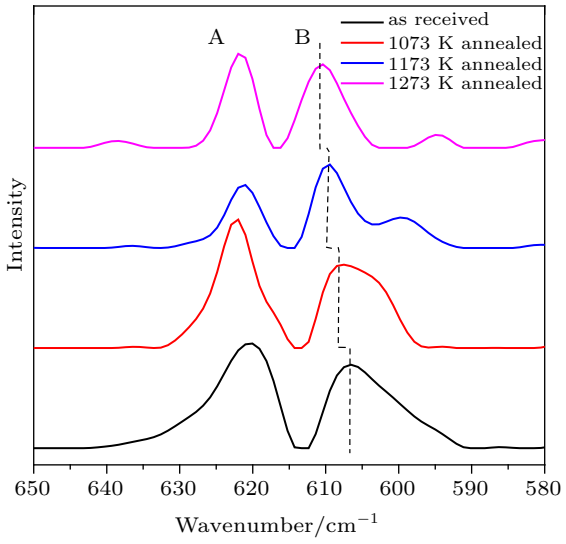


Fig. 2. (color online) FTIR spectra of the annealed $SrTiO_3$ samples, compared with that of as-received $SrTiO_3$ sample. For easy comparison, the spectra were shifted vertically.

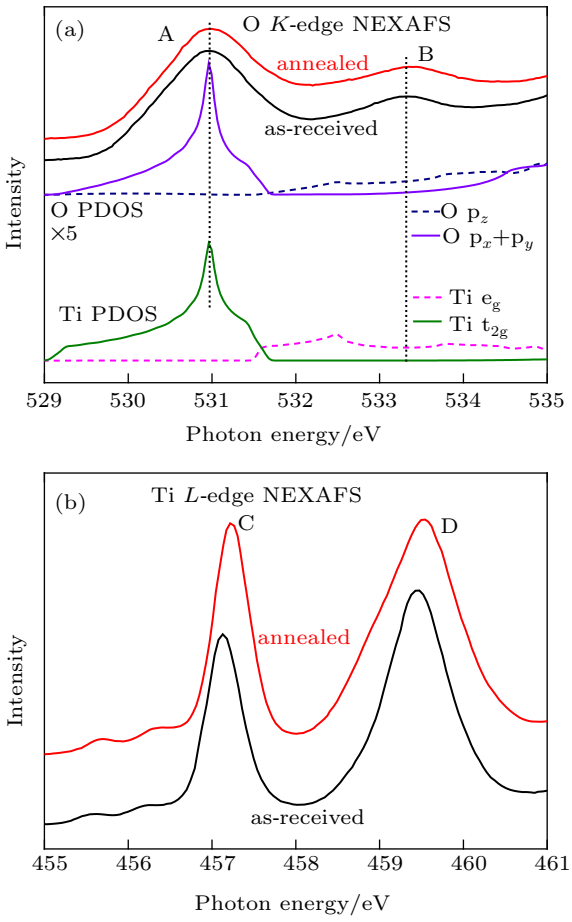


Fig. 3. (color online) (a) O *K*-edge and (b) Ti *L*-edge NEXAFS spectra of the annealed $SrTiO_3$ sample, compared with as-received $SrTiO_3$ sample. The calculated O 2p and Ti 3d PDOS of $SrTiO_3$ is shown in panel (a) as reference.

Meanwhile, the intensity ratio between peaks A and B is reduced after annealing. Similar results have been reported for an oxygen-deficient system.[29] Such change can be associated with the filling of the low energy t_{2g} band (hence, reducing the density of the unoccupied states) by the excess electrons due to the oxygen vacancies. To further confirm the presence of the oxygen vacancies, the Ti L_3-edge NEXAFS spectrum of the annealed sample is shown in Fig. 3(b) as well as that of the as-received sample. The peaks C at 457.1 eV and D at 459.4 eV are originated from the transitions from the Ti $2p_{3/2}$ core level to the unoccupied Ti 3d bands (t_{2g} and e_g, respectively). A slight broadening of the peaks is observed in the spectra of the annealed samples. This is likely contributed by the presence of Ti 3+ state.[29] In the oxygen-deficient $SrTiO_3$ system, each oxygen vacancy provides two electrons to the Ti d band, leading to a reduction of the Ti from 4+ to partial 3+ state.

Based on the FTIR and NEXAFS results, we propose a structure evolution model to explain the thermal conductivity reduction mechanism. First, annealing induces a reordering process for the atoms in some areas. Therefore, within the areas, the atoms line up in a better order, which improves the overall crystal quality. However, this leads to a more disorder/imperfect structure, such as oxygen vacancies, at the regions between the areas. Second, the samples annealed with reduced oxygen pressure may yield a large amount of oxygen vacancies. For example, the sample that has been annealed in the Ar atmosphere for 24 h shows chain-like features (observed on the SEM image, S.I.-1), which is consistent with other reports.[30,31] Thus, the change in thermal conductivity may result from a competition between the crystallization inside some domains and the increased imperfection scattering in the region between these domains.

To quantitatively evaluate the proposed model, a phenomenological Callaway's model[32–37] is used to fit the thermal conductivity data (shown in Fig. 1). In this model, the lattice thermal conductivity is given by

$$\kappa = \frac{k_B}{2\pi^2 v_s}\left(\frac{k_B T}{\hbar}\right)^3 \int_0^{\theta_D/T} \tau(x)\frac{x^4 e^x}{(e^x-1)^2}\,dx, \qquad (2)$$

where $x = \hbar\omega/k_B T$ is the reduced phonon frequency, θ_D is the Debye temperature, and v_s is the velocity of sound.[32–37] Callaway's model assumes that the phonon dispersion has a Debye spectrum and the relaxation time representing different scattering process follows Matthiessen's rule. Since the system in our study is a single crystal, the dominant scattering processes are phonon–phonon Umklapp scattering and point defect scattering (could be from oxygen vacancy or other imperfection)

$$\tau_U^{-1} = S_0 T\omega^2 = Ex^2, \qquad (3)$$

$$\tau_{PD}^{-1} = A\omega^4 = Dx^4, \qquad (4)$$

where S_0 and A are constant parameters characteristic of each sample and reflect the strengths of the phonon–phonon U scattering process and the point defect, respectively. The thermal conductivity modeled by the Callaway's equation shows relatively good agreement with the experimental results (shown in Appendix Fig. A2). Both the S_0 and A values increase with increasing annealing temperature, as listed in Table 1. Such results can be understood when we further examine the relationship between the S_0 and A values and the concentration of defects. The phonon–phonon scattering parameter S_0 is given by the following equation:

$$S_0 = \frac{2\gamma^2 k_B}{\mu V_0 \omega_D}, \qquad (5)$$

where γ is the Grüneisen parameter, μ is the shear modulus, V_0 is the volume per atom, and ω_D is the Debye frequency.[37] The segregation of defects generally leads to the degradation of materials' strength (e.g., shear modulus). At the same time, other parameters in Eq. (5) are less sensitive to the segregation of defects. Hence, the reduction of shear modulus due to the rise of defect concentration and the segregation of defects overwhelms the change of other factors in the equation, which results in an increase of S_0. On the other hand, the point defect scattering parameter A is given by Klemens[35] as

$$A = \frac{V}{4\pi v_s^3}\Gamma, \qquad (6)$$

where V is the volume per atom, and v_s is the phonon velocity. The parameter Γ is related to the defect concentration and the phonon scattering strength and consists of mass fluctuation and strain field terms,[36] which can be calculated by the following formula:

$$\Gamma = \Gamma_{MF} + \Gamma_{SF} = \sum_i x_i\left[\left(\frac{\Delta M_i}{M}\right)^2 + \varepsilon\left(\frac{\Delta\delta_i}{\delta}\right)^2\right], \qquad (7)$$

where Γ_{MF} and Γ_{SF} represent the point scattering related to mass fluctuation scattering and strain field scattering, respectively. ΔM is the mass difference between the host and the impurity atoms, M is the average mass, ε is a phenomenological parameter related to the strain, $\Delta\delta_i$ is the difference in ionic radius between the host and the impurity atoms, and δ is the average ionic radius. Both the mass fluctuation and strain field due to the vacancy site are linearly proportional to the density of the oxygen vacancies. Hence, the significant increase in A after annealing indicates a large increase of the oxygen vacancy concentration after annealing, which is consistent with the observation in experimental measurement.

Table 1. Fitted scattering parameter S_0 and A for annealed sample compared with that for as-received sample.

Sample	$S_0/10^{-19}$ s·K^{-1}	$A/10^{-41}$ s^3
As received	0.95	1.96
1073 K annealed	0.99	3.65
1273 K annealed	1.32	2.53
1473 K annealed	1.50	2.61

The LFA has been used to investigate the phonon scattering in lead chalcogenide thermoelectric[5,37] and the thermal characterization of a bridge-link carbon nanotubes array used as a thermal adhesive.[38] More recently, we used combined SEM, LFA, DSC, and finite element method to investigate the thermal properties of boron nitride, and demonstrated that hexagonal boron nitride laminates exhibit a high thermal conductivity, which is significantly larger than that currently used in thermal management.[39] With additional characterizing methods (such as FTIR and NEXAFS) included, this work successfully demonstrates the usefulness of the integrated study of several tools to reveal the origin of reduced thermal conductivity in annealed $SrTiO_3$. It is clearly shown that the unique advantage of the combined methods can be achieved because the different aspects of functional materials can be investigated by different characterization means. For example, the thermal transport properties such as thermal diffusivity can be characterized by LFA, the heat capacity can be obtained by DSC measurement, and the mechanism of thermal conductivity can be analyzed by Callaway's model. The crystal structure can be observed by SEM, the vibrational properties can be determined by FTIR, and the electronic properties can be revealed by near edge x-ray absorption fine structure and first-principles calculations. The whole picture of the crystal structure of the material and its properties can then be obtained. The combined method, as proposed in this work, is expected to be useful to study other advanced functional materials.

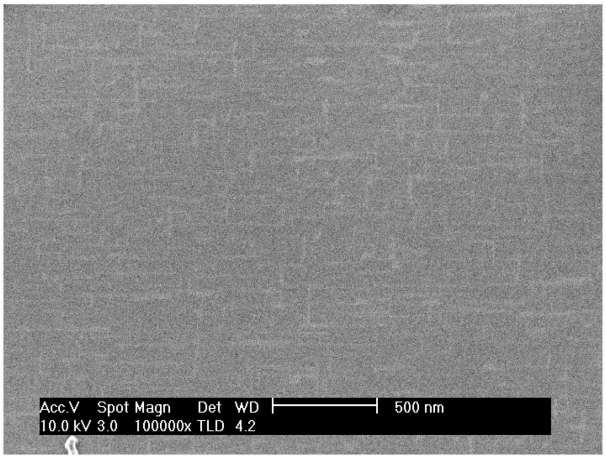
4. Conclusion

$SrTiO_3$ samples were annealed at various temperatures either in Ar atmosphere or under vacuum. Based on the experimentally measured thermal diffusivity and specific heat, the thermal conductivity of the samples was calculated, which dramatically decreased with increasing annealing temperature. The FTIR and NEXAFS reveal that the defects (i.e., oxygen vacancies) in the samples increase (especially after being annealed under vacuum) and segregate after annealing, which is consistent with the change of the morphology of the samples and other reported results. A phenomenological model based on Callaway's theory was used to fit the thermal conductivity of the samples. The results confirm that the increasing annealing temperature leads to an increase and segregation of oxygen vacancies, which is responsible for the significant reduction of the thermal conductivity after annealing. This work demonstrates the unique usefulness of the integrated study for revealing the mechanism of thermal conductivity of $SrTiO_3$. Therefore, this work suggests a promising means to characterize and optimize the material for thermoelectric applications.

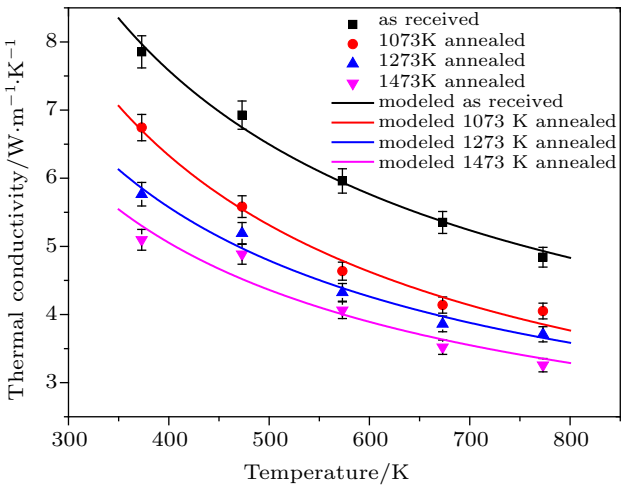
Acknowledgment

The authors are particularly grateful to Yu Chiuan Li, Chia-Hsin Wang, Yaw-Wen Yang, Kuan Chang Chang, Ting Chang Chang, and Tsun Ming Tsai for their valuable assistance. This part has been financially supported by the Robert-Bosch Stiftung (Sustainable Partners project No. 32.05.8003.0112.0), the Impuls- und Vernetzungsfonds of the Helmholtz-Association (Grant No. VH-NG-423).

Appendix A



A1. SEM image of $SrTiO_3$ annealed in Ar atmosphere showing linear dislocations.



A2. (color online) Thermal conductivity of annealed $SrTiO_3$ compared with that of as received $SrTiO_3$. The dots represent the experimental values and lines are values modeled using Callaway's equation.

References

[1] DiSalvo F J 1999 *Science* **285** 703
[2] Snyder G J and Toberer E S 2008 *Nat. Mater.* **7** 105
[3] Zheng J C 2008 *Front. Phys. China* **3** 269
[4] Fan Z, Zheng J, Wang H Q and Zheng J C 2012 *Nanoscale Res. Lett.* **7** 570
[5] He J, Zhao L D, Zheng J C, Doak J, Wu H, Wang H Q, Lee Y, Wolverton C, Kanatzidis M G and Dravid V P 2013 *J. Am. Chem. Soc.* **135** 4624
[6] Ohta S, Nomura T, Ohta H and Koumoto K 2005 *J. Appl. Phys.* **97** 034106

[7] Ravichandran J, Siemons W, Oh D W, Kardel J T, Chari A, Heijmerikx H, Scullin M L, Majumdar A, Ramesh R and Cahill D G, 2010 *Phys. Rev. B* **82** 165126

[8] Zhao L D, Lo S H, Zhang Y, Sun H, Tan G, Uher C, Wolverton C, Dravid V P and Kanatzidis M G 2014 *Nature* **508** 373

[9] Okuda T, Nakanishi K, Miyasaka S and Tokura Y 2001 *Phys. Rev. B* **63** 113104

[10] Foley B M, Brown-Shaklee H J, Duda J C, Cheaito R, Gibbons B J, Medlin D, Ihlefeld J F and Hopkins P E 2012 *Appl. Phys. Lett.* **101** 231908

[11] Bhattacharya S, Dehkordi A M, Tennakoon S, Adebisi R, Gladden J R, Darroudi T, Alshareef H N and Tritt T M 2014 *J. Appl. Phys.* **115** 223712

[12] Popuri S R, Scott A J M, Downie R A, Hall M A, Suard E, Decourt R, Pollet M and Bos J W G 2014 *RSC adv.* **4** 33720

[13] Muta M, Kurosaki K and Yamanaka S 2005 *J. Alloy. Comp.* **392** 306

[14] Yu C, Scullin M L, Huijben M, Ramesh R and Majumdar A 2008 *Appl. Phys. Lett.* **92** 191911

[15] Li F, Chen J W, Chen J H, *et al.* 2015 *Acta Phys. Sin.* **64** 198801 (in Chinese)

[16] Yu H S, Xia H L, Hu W, *et al.* 2015 *Acta Phys. Sin.* **64** 217402 (in Chinese)

[17] Zhu Hui-Long, Luo Wei-Chun, Wang Yan-Rong, *et al.* 2015 *Chin. Phys. B* **24** 117306

[18] Wang T, Cheng Y, Sun Y J, *et al.* 2015 *Chin. Phys. B* **24** 107303

[19] Qiu R, Gao X, Jiang Y, *et al.* 2016 *Acta Phys. Sin.* **65** 044209 (in Chinese)

[20] Parker W J, Jenkins R J, Butler C P and Abbott G L 1961 *J. Appl. Phys.* **32** 1679

[21] Blaha P, Schwarz K, Madsen G K H, Kvasnicka D and Luitz J 2001 *WIEN2k, An Augmented Plane Wave Plus Local Orbitals Program for Calculating Crystal Properties,* Vienna University of Technology, Vienna, Austria

[22] Sjöstedt E, Nordstrom L and Singh D J 2000 *Solid State Commun.* **114** 15

[23] Perdew J P, Burke K and Ernzerhof M 1996 *Phys. Rev. Lett.* **77** 3865

[24] Perry C H, Khanna B N and Ruppecht G 1964 *Phys. Rev.* **135** 408

[25] Gervais F, Servoin J L, Baratoff A, Bednorz J G and Bining G 1993 *Phys. Rev. B* **47** 8187

[26] de Groot F M F, Faber J, Michiels J J M, Czyzyk M T, Abbate M and Fuggle J C 1993 *Phys. Rev. B* **48** 2074

[27] Muller D A, Nakagawa N, Ohtomo A, Grazul J L and Hwang H Y 2004 *Nature* **430** 657

[28] Browning N D, Moltaji H O and Buban J P 1998 *Phys. Rev. B* **58** 8289

[29] Lusvardi V S, Barteau M A, Chen J G, Eng Jr. J, Frühberger J and Teplyakov A 1998 *Surf. Sci.* **397** 237

[30] Liao X X, Wang H Q and Zheng J C 2013 *J. Am. Ceram. Soc.* **96** 538

[31] Szot K, Specier W, Carius R, Zastrow U and Beyer W 2002 *Phys. Rev. Lett.* **88** 075508

[32] Callaway J 1959 *Phys. Rev.* **113** 1046

[33] Callaway J 1960 *Phys. Rev.* **120** 1149

[34] Zou J, Kotchetkov D, Balandin A A, Florescu D I and Pollak F H 2002 *J. Appl. Phys.* **92** 2534

[35] Klemens P G 1955 *Proc. Phys. Soc. London A* **68** 1113

[36] Abeles B 1963 *Phys. Rev.* **131** 1906

[37] He J Q, Girard S N, Zheng J C, Zhao L D, Kanatzidis M G and Dravid V P 2012 *Adv. Mater.* **24** 4440

[38] Hao R, Lin W Q, Zheng J C and Lu M 2014 *Int. J. Adhesion and Adhesives* **49** 58

[39] Zheng J C, Zhang L, Kretinin A V, Morozov S V, Wang Y B, Wang T, Li X, Ren F, Zhang J, Lu C Y, Chen J C, Lu M, Wang H Q, Geim A K and Novoselov K S 2016 *2D Materials* **3** 011004